

- 27, L91 (1988).
97. B-Y. Tsauro, M. S. Dilorio, A. J. Strauss, *Appl. Phys. Lett.* **51**, 858 (1987).
  98. Z. L. Bao *et al.*, *ibid.*, p. 946.
  99. M. Naito *et al.*, *J. Materials Res.* **2**, 713 (1987).
  100. A. Mogro-Campero, L. G. Turner, *Appl. Phys. Lett.* **52**, 1185 (1988).
  101. K. Char, A. D. Kent, A. Kapitulnik, M. R. Beasley, T. H. Geballe, *ibid.* **51**, 1370 (1987).
  102. M. Scheuermann *et al.*, *ibid.*, p. 1951.
  103. R. E. Somekh *et al.*, *Nature* **326**, 857 (1987).
  104. R. M. Silver, J. Talvacchio, A. L. deLozanne, *Appl. Phys. Lett.* **51**, 2149 (1987).
  105. T. Aida, T. Fukazawa, K. Takagi, K. Miyauchi, *Jpn. J. Appl. Phys.* **26**, L1489 (1987).
  106. J. L. Makous *et al.*, *Appl. Phys. Lett.* **51**, 2164 (1987).
  107. M. Hong, S. H. Liou, J. Kwo, B. A. Davidson, *ibid.*, p. 694.
  108. H. Adachi, K. Hirochi, K. Setsune, M. Kitabatake, K. Wasa, *ibid.*, p. 2263.
  109. H. Asano, K. Tanabe, Y. Katoh, S. Kubo, O. Michikami, *Jpn. J. Appl. Phys.* **26**, L1221 (1987).
  110. H. C. Li, G. Linker, F. Ratzel, R. Smithy, G. Geerk, *Appl. Phys. Lett.* **52**, 1098 (1988).
  111. G. K. Wehner, Y. H. Kim, D. H. Kim, A. M. Goldman, *ibid.*, p. 1187.
  112. D. Dijkkamp *et al.*, *ibid.* **51**, 619 (1987).
  113. J. Narayan, N. Biunno, R. Singh, O. W. Holland, O. Auciello, *ibid.*, p. 1845.
  114. A. M. DeSantolo, M. L. Mandich, M. F. Jarrold, J. E. Bower, S. Sunshine, in *Thin Film Processing and Characterization of High Temperature Superconductors*, AIP Conference Proceedings No. 165, J. Harper, R. Colton, and L. Feldman, Eds. (American Institute of Physics, New York, 1988), pp. 174–181.
  115. O. Auciello, A. R. Krauss, J. Santiago-Aviles, A. F. Schreiner, D. M. Gruen, *Appl. Phys. Lett.* **52**, 239 (1987).
  116. C. E. Rice, R. B. VanDover, G. J. Fisanick, *ibid.* **51**, 1842 (1987).
  117. M. E. Gross, M. Hong, S. H. Liou, P. K. Gallagher, J. Kwo, *ibid.* **52**, 160 (1988).
  118. S. M. Sze, Ed., *VLSI Technology*, (McGraw-Hill, New York, 1983).
  119. S. Matsui, N. Takado, H. Tsuge, K. Asakawa, *Appl. Phys. Lett.* **52**, 69 (1988).
  120. G. J. Clark, F. K. LeGoues, A. D. Marwick, R. B. Laibowitz, R. Koch, *ibid.* **51**, 1462 (1988).
  121. G. J. Fisanick *et al.*, in *Thin Film Processing and Characterization of High Temperature Superconductors*, AIP Conference Proceedings No. 165, J. Harper, R. Colton, L. Feldman, Eds. (American Institute of Physics, New York, 1988), pp. 189–196.
  122. A. Inam *et al.*, *Appl. Phys. Lett.* **51**, 1112 (1987).
  123. M. Scheuermann *et al.*, *ibid.*, p. 1951.
  124. T. Van Duzer and C. W. Turner, *Principles of Superconductive Devices and Circuits* (Elsevier, New York, 1981).
  125. R. B. VanDover, A. De Lozanne, R. E. Howard, W. L. McLean, M. R. Beasley, *Appl. Phys. Lett.* **37**, 838 (1980).
  126. A. D. Wieck, *ibid.* **52**, 1017 (1988).
  127. J. W. Ekin *et al.*, *ibid.*, p. 1819.
  128. P. M. Mankiwich *et al.*, in *Extended Abstracts of the Topical Meeting on High-Temperature Superconducting Electronic Devices*, June 1988, Miyagi-Zao, Japan (Research and Development Association for Future Electronic Devices, Tokyo, Japan), pp. 157–160.
  129. We thank all of our colleagues at AT&T Bell Laboratories for continued collaborations and valuable discussions. We especially thank J. Thomson, D. Lishner, and R. Stanton for preparation of the screen-printed materials and W. W. Rhodes for the tape-cast material, and P. M. Mankiwich for helpful suggestions to this paper. We also thank our scientific colleagues over the world for sharing their preprints with us.

# Synthesis of Buried Oxide and Silicide Layers with Ion Beams

ALICE E. WHITE AND K. T. SHORT

**Ion implantation, because it is inherently a strongly nonequilibrium process, can add a new dimension to materials studies. A large variety of chemical elements may be readily introduced into a target substrate by ion bombardment at concentrations considerably greater than the normal solid solubilities. In addition, the interaction of the accelerated ions with the target produces lattice defects. Both effects have been studied extensively in experiments directed at understanding the mechanisms of formation of buried oxide and silicide layers in silicon with high-dose ion implantation. These layers have properties that are difficult to attain with conventional techniques.**

EXPERIMENTS IN ION IMPLANTATION WERE FIRST PERFORMED almost 40 years ago by nuclear physicists (1). More recently, ion implanters have become permanent fixtures on the processing lines of integrated circuits. Manufacture of the more complex chips may involve as many as ten different ion implantation steps. Implantation is used primarily at fluences of  $10^{12}$  to  $10^{13}$  ions/cm<sup>2</sup> to tailor the electrical properties of a semiconductor substrate. Figure 1A shows a cross-sectional view of a typical complementary metal-oxide-semiconductor (CMOS) device structure consisting of both *n*- and *p*-channel MOSFETs (MOS field effect transistors) (2, 3). Other conventional uses of implantation in semiconductors include amorphization for isolation [particularly in

gallium arsenide (GaAs) circuits] (4) and for fundamental solid-state studies (5) and mixing of multilayer films for phase formation (6). Implantation of nitrogen into metals has been used since the early 1970s to improve the corrosion and wear resistance of base metals such as steel (7) and has been exploited in the manufacture of bearings, artificial joints, and stamping punches and dies. In the past, applications of implantation were limited by the small beam currents that were available, but recently a new generation of high-current implanters has entered the market. This high current capability allows us to implant the extremely large concentrations required for our work on compound synthesis—in some cases five orders of magnitude higher than those required for doping.

The small fluences required by most conventional applications of implantation represent an almost negligible perturbation in the composition of the target (<1 atomic %). In general, the concentrations of implanted ions are so small that they are hard to detect directly with most analysis techniques, and the damage to the crystalline lattice may be used as the earmark of the implant. In this article, we consider implantation that significantly alters the composition of the target, specifically implantation of enough ions to create a compound. Typical solids have densities of  $\sim 5 \times 10^{22}$  atoms/cm<sup>3</sup>, so formation of a compound AB, where B is the substrate material, would require a fluence of  $\sim 2.5 \times 10^{17}$  ions/cm<sup>2</sup> for a 1000-Å layer. If the doping implantations take about 1 min to complete, these implantations would take 2 months at the usual implanter beam current. Higher currents are therefore essential.

The authors are at AT&T Bell Laboratories, Murray Hill, NJ 07974.

## The Implantation Process in Semiconductors

The implantation process for a single ion impinging on a semiconductor substrate is illustrated in Fig. 1B. The ion is accelerated to  $\sim 200$  keV, enters the substrate, and eventually comes to rest by losing energy through a combination of collisions with the lattice atoms (nuclear stopping) and drag from the lattice electrons (electronic stopping) (7). The atoms with which it comes in contact can be displaced from their lattice sites by the force of the collision and can, in turn, experience collisions. This trail of destruction has been studied with analytical techniques as well as with Monte Carlo simulations (8). Additional ions striking the target create their own collision cascades, generating vacancies and interstitials, until eventually the damaged regions overlap. For semiconductors, this can completely destroy the crystalline order, rendering the material amorphous. If the substrate temperature is elevated above room temperature, considerable healing of the implant damage occurs during the implant. This is called dynamic annealing. The final depth profile of the implanted ions is approximately Gaussian, with the peak concentration occurring at a depth determined by the atomic number ( $Z$ ), the mass, and the energy of the implanted ion as well as the atomic number and mass of the target. One of the reasons implantation is so useful in semiconductor technology is that the damaged region can be recrystallized by annealing, with the substrate used as a seed. For most dopants at low concentrations,

almost perfect regrowth of the substrate (less than  $10^3$  residual defects per square centimeter) and activation of the dopants can be achieved.

Despite years of experience, the production of ion beams still involves art as well as science. In our system, the ion beams are produced in the source region of an implanter by a high current discharge to a hot cathode in an arc chamber which generates a plasma of charged ions. The ion species is introduced by bleeding a gas into the chamber or by heating a solid source until its vapor pressure is  $\sim 1 \times 10^{-4}$  torr. If the plasma can be stabilized, the ions are extracted with a negative voltage (40 kV for our machine) and analyzed with a magnet to select a desired isotope. This mass-selected beam is then accelerated to the desired energy ( $\leq 200$  keV for our system) before being focused and directed by electromagnetic lenses. Because the beam cannot be seen, the implanter operator relies on a few diagnostics of the beam current to follow its progress. An aperture on the arc chamber determines the initial shape of the beam (millimeters in size), but it is usually raster-scanned over an aperture located at the target to achieve uniform large-area coverage. One then measures the concentration of implanted ions by collecting the current deposited on the target, taking care to collect all incident ions and scattered products. The high currents that we use cause increased target heating. This is an important consideration; the power deposited by a 200-keV,  $10\text{-}\mu\text{A}/\text{cm}^2$  beam into a 10-cm-diameter silicon (Si) wafer is sufficient to raise the temperature to  $400^\circ\text{C}$ . Fortunately, these problems are not intractable.

Since ion ranges for typical dopant ions in Si are tenths of micrometers, a subsurface analysis technique is needed to characterize samples. Transmission electron microscopy (TEM) provides structural information, and secondary ion mass spectrometry (SIMS) and Auger depth profiling give compositional information; however, the sample is destroyed during these measurements. We find that Rutherford backscattering spectroscopy (RBS), where the sample is bombarded with a helium beam (2-MeV  $\text{He}^+$  beam) and the He ions that are scattered back at  $\sim 180^\circ$  are collected, has several advantages as a survey technique: (i) it provides quantitative information about composition as a function of depth, (ii) the sampling depth is on the order of a micrometer, (iii) there is virtually no sample preparation required, (iv) collection of a spectrum usually takes less than 30 min, and (v) it is nondestructive. In addition, if the major crystallographic axes of the substrate are aligned with the incoming  $\text{He}^+$  beam, the backscattered yield (referred to as the "channeled" yield) is reduced but displaced lattice atoms are highlighted, so information about defects such as interstitials and dislocations can be obtained (9). A typical spectrum consists of a plot of the output of a multichannel analyzer, which measures the yield of backscattered ions as a function of their energy (where lower energy corresponds to lower target mass or deeper probing).

Some fascinating new effects emerge when high-fluence implantation is used to alter the chemical composition of a target. The formation of buried oxide layers in Si is used as an example in the next section. This technique has interesting technological implications. We have extended this work to looking at narrow oxide layers, which provided some unexpected insights for our current research on the formation of buried single-crystal silicide layers.

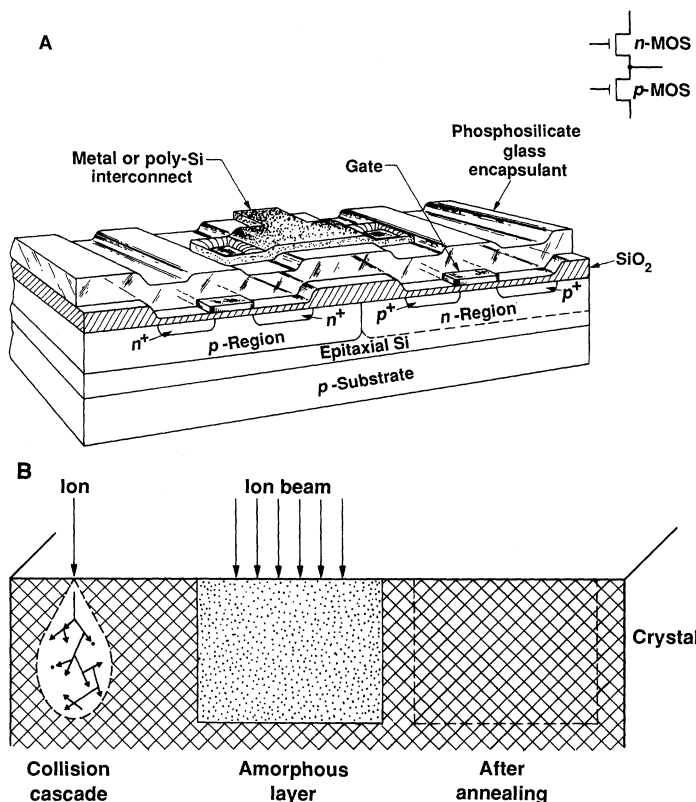


**Fig. 1.** (A) Drawing of the structure of a CMOS device with both  $n$ - and  $p$ -channel MOSFETs, showing a typical use of implantation in integrated circuit fabrication. The devices are fabricated in a layer of epitaxial Si grown on a Si wafer with a background  $p$ -type doping. The  $n^+$  contacts are formed by implantation with either phosphorus, arsenic, or antimony at concentrations of  $\sim 10^{18}$  ions/ $\text{cm}^3$ . Similarly, the  $p^+$  contacts are implanted with boron to  $10^{18}$  ions/ $\text{cm}^3$ . The contacts are defined laterally by masking with photoresist or  $\text{SiO}_2$  and vertically by careful selection of the implant energy. (B) Schematic of the implantation process, which starts with a single ion entering a crystalline substrate and generating collision cascades. Overlapping cascades may eventually create an amorphous region, but this can often be recrystallized by a relatively low-temperature furnace anneal ( $\sim 600^\circ\text{C}$ ).

## Mechanisms of Formation of Buried Oxide Layers

The first reports of buried silicon dioxide ( $\text{SiO}_2$ ) layers fabricated by ion implantation of oxygen (O) appeared over 10 years ago (10). This technique was quickly exploited by Izumi *et al.*, who demon-

strated high-performance CMOS ring oscillators in a SIMOX (separation by implantation of oxygen) wafer (11). Since then, it has been an active area of research with several groups investigating its viability as a Si-on-insulator (SOI) technology; considerable progress has been made in creating useful structures (12). Competing SOI technologies include growth of Si on sapphire (SOS) and zone-melting recrystallization (ZMR) (13). At the fall 1987 meeting of the Materials Research Society, Chen reported fabrication of 4-kbyte static random access memory (SRAM) chips with a 2.5- $\mu\text{m}$  linewidth on SIMOX wafers, which showed bulk mobilities and leakage currents less than  $10^{-13}$  A/ $\mu\text{m}^2$  (14).

Most of the early work involved  $\text{O}^+$  fluences of about  $2 \times 10^{18}$  ions/ $\text{cm}^2$ , large enough to create a layer of stoichiometric  $\text{SiO}_2$  by the end of the implantation. When these layers are heat-treated at temperatures above  $1200^\circ\text{C}$ , the edges of the O implant profile (which saturates when the stoichiometric concentration of O is achieved) become steeper and the damage in the surface Si is partially healed. Because our interest is in understanding the driving forces behind the layer growth, we used substoichiometric implants in which the peak concentration of implanted O is below that required for  $\text{SiO}_2$  (67 atomic %) (15). The ions are deposited in an approximately Gaussian profile that is buried beneath the Si surface. When such a sample is annealed in a furnace at  $1400^\circ\text{C}$  (near the  $1410^\circ\text{C}$  melting point of Si) for  $\sim 30$  min, a dramatic transformation takes place. The O in the tails of the implant profile travels up the concentration gradient, driven by the chemical potential, to form a narrow, well-defined layer of stoichiometric amorphous  $\text{SiO}_2$ . Advantages of this approach are that the lower concentrations mean shorter implantation times and fewer defects in the surface Si. In addition, it is easier to observe the process of layer formation unobscured by a thick amorphous  $\text{SiO}_2$  layer.

This transformation can be readily seen in the RBS spectra from a typical buried oxide specimen before and after annealing (Fig. 2, A and B). This thin buried oxide layer was formed by implanting 170-keV  $\text{O}^+$  ions into a Si wafer to a fluence of  $3 \times 10^{17}$  ions/ $\text{cm}^2$ . Instead of studying the O region of the spectrum, which appears on top of the long tail from the Si substrate, we focus on the decrease in intensity at 0.95 MeV in the Si spectrum. This decrease is the yield deficit in the Si due to the presence of so much O and it exhibits the expected Gaussian shape. The peak of the Gaussian implant profile occurs at a depth of  $\sim 3700$  Å and has a spread (called the straggle) of  $\pm \sim 1000$  Å. The O concentration at the peak is 21 atomic %, significantly below the 67 atomic % required to form  $\text{SiO}_2$ . If the wafer is held at a slightly elevated temperature during the implant, dynamic annealing ensures that the surface Si is not completely disordered. Comparing the random and channeled yield in the surface Si in the unannealed case (Fig. 2A) shows that, although heavily damaged, some axial alignment of the surface Si is retained. After the heat treatment (Fig. 2B), the O coalesces into a layer and, in addition, the Si crystal regrows, using the substrate and the surface as seeds. This recrystallization is seen as a reduction of the channeling yield of the surface Si in Fig. 2B to a level corresponding to the sensitivity limit of RBS (9). Indeed, if the surface Si is completely amorphized by the beam, it becomes polycrystalline during the anneal. However, the channeling yield in the Si increases on both sides of the buried oxide layer, which indicates some sort of residual damage.

Investigation of this sample with TEM provides more information about the microstructure. If the sample is cleaved perpendicular to the surface and then thinned, a cross-sectional view of the layer is obtained (Fig. 3A). As anticipated from the RBS results, we see a narrow, continuous oxide layer with abrupt interfaces buried under  $\sim 3400$  Å of Si. Although the top 1500 Å of Si has no observable defects (corresponding to an upper bound of  $10^8$  defects

per square centimeter), there are asymmetric bands of crystalline defects on either side of the layer. These are twinned regions of the crystal where the regrowth occurs in opposite directions. Monte Carlo calculations (8) suggest that the bands are centered on the peak of the damage caused by the implant, which falls forward of the peak of the O concentration. The twins are definitely cause for concern, since defect states at the Si/ $\text{SiO}_2$  interface can trap carriers, but they can be readily eliminated by a low-dose Si implant that serves to reamorphize the twinned region, followed by a gentle anneal at  $600^\circ\text{C}$ , which gives the Si a chance to recrystallize uniformly (16).

In order to probe the details of this layer formation process, we decided to vary the degree of dynamic annealing by varying the substrate temperature, which had a profound effect on the morphology of the final layer, as illustrated in Fig. 3B for a 1-MeV implant performed at  $500^\circ\text{C}$  on a Van de Graaff accelerator. What looked to be a smooth, Gaussian-shaped implant profile in RBS (similar to Fig. 2A) turned out to have interspersed bands of crystalline and amorphous material when viewed by high-resolution TEM. During

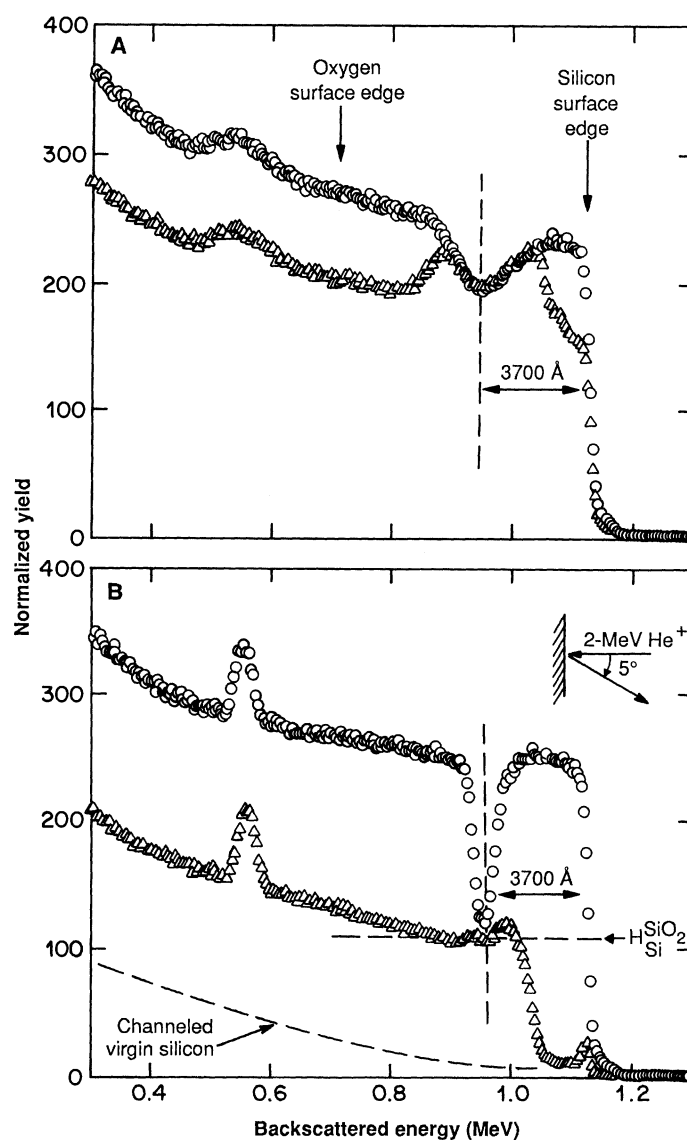


**Fig. 2.** (A) Random (circles) and channeled (triangles) RBS spectra for a 170-keV  $\text{O}^+$  implant ( $3 \times 10^{17}$  ions/ $\text{cm}^2$ ) at  $\sim 100^\circ\text{C}$ . The backscattered energy corresponding to surface Si and O are indicated by downward-pointing arrows. (B) RBS spectra from the sample in (A) after annealing at  $1390^\circ\text{C}$  for 30 min. [Reprinted from (21) with permission © *Applied Physics Letters*]

the subsequent high temperature anneal, the amorphous regions (which are evidence for premature segregation of O during the implant) coalesce, isolating islands of Si in the growing oxide layer. Because Si does not readily diffuse in SiO<sub>2</sub>, these islands are trapped and they are responsible for the lumpy appearance of the layer in Fig. 3B. This was particularly easy to observe in our substoichiometric layers, but similar islands are also seen at the edges of thicker layers (17).

After we had studied the results of this experiment, it became clear that we were observing a classical competition between nucleation and growth of precipitates similar to what is seen in thin film growth. In this case, the kinetics of precipitate growth are determined by balancing the energetically favorable formation of new SiO<sub>2</sub> and the energetically unfavorable increases in surface tension. At low substrate temperatures, the damage from the ion beam creates a myriad of nucleation sites leading to homogeneous nucleation of SiO<sub>2</sub> precipitates and uniform oxide layer growth. Twins are the unfortunate side effect. Higher substrate temperatures solve the twin problem but favor growth of a limited number of nuclei, resulting in nonuniform growth and discontinuous layers.

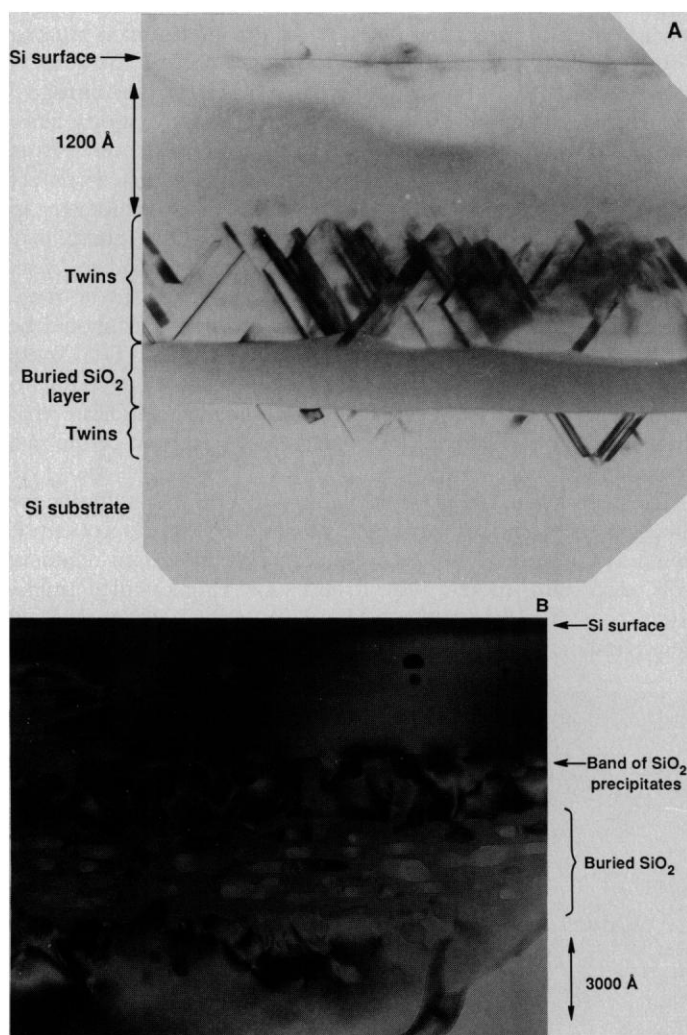


**Fig. 3.** (A) TEM micrograph of the 600 Å buried oxide layer from Fig. 2B showing the asymmetric bands of twins. (B) Oxide layer formed from a 1-MeV O<sup>+</sup> implant of  $8 \times 10^{17}$  ions/cm<sup>2</sup> at elevated temperature (500°C) after annealing at 1390°C for 15 min. Premature segregation of O during the implant leads to isolation of Si islands in the growing layer. In addition, a band of SiO<sub>2</sub> precipitates becomes stranded at a depth corresponding to the peak of the damage from the implant. It is difficult to improve this structure by annealing. [Reprinted from (15) with permission © *Applied Physics Letters*]

The driving force behind this process seems to be the large gain in free energy by formation of SiO<sub>2</sub>. Silicon nitride (Si<sub>3</sub>N<sub>4</sub>), which also has a large heat of formation, has been fabricated with implantation and annealing (18). Therefore, we decided to attempt to fabricate the silicides (compounds of metals with Si), which have heats of formation that are smaller by at least a factor of 2 than that of SiO<sub>2</sub> (19), in order to determine the generality and limitations of the process. In addition to being good conductors with high mechanical and thermal stability, the silicides are easy to etch and they are stable in oxidizing environments. For these reasons, they are very compatible with Si processing and have great technological relevance. Moreover, many of the metal disilicides have a lattice spacing that is near that of Si. One advantage is that we only need to implant one metal ion for every two Si atoms to reach stoichiometry; the drawbacks are that the heavier ions mean shallower implant depths and more damage.

### Mesotaxy: Single-Crystal Growth of Buried Disilicide Layers

The conventional process for growing silicides involves deposition of a metal film, usually in ultrahigh vacuum (UHV,  $<10^{-10}$  torr), followed by reaction at  $\sim 600^\circ\text{C}$  to form the silicide. This process results in extremely high-quality epitaxial films with smooth interfaces on Si wafers oriented with (111) planes parallel to the surface; however, the films are difficult to grow this way on the more common (100) orientation of silicon (20). Using high-dose implantation, we have succeeded in making in both (111) and (100) Si buried single-crystal silicide layers with electrical characteristics that are better than those of the best vapor-deposited films and comparable to or better than the electrical characteristics of the bulk (21). We call this technique "mesotaxy" for oriented growth inside the substrate, as contrasted with epitaxial growth on the surface.

Our first experiments were with cobalt disilicide (CoSi<sub>2</sub>), because much is known about thin film growth of this material. It has the CaF<sub>2</sub> structure and a small lattice mismatch with Si,  $\sim 1.2\%$  at room temperature. For mesotaxy, we implanted 200-keV Co<sup>+</sup> ions which created an approximately Gaussian profile beneath the surface of a Si wafer that was held at elevated temperature. This structure was not entirely expected, however. Normally, such high doses of heavy elements would cause large numbers of the target atoms to be ejected, resulting in significant erosion (sputtering) of the surface and an implant profile that is no longer buried (22). Earlier attempts to implant transition metals at high doses confirmed these expectations, even when the substrate temperature was elevated (23). One reason this experiment was successful was that the implant concentration was held to  $3 \times 10^{17}$  ions/cm<sup>2</sup> (we had evidence that substoichiometric doses were adequate for layer formation).

Both RBS and channeling were used to monitor the samples before and after annealing. Results from a sample implanted at 350°C show that the Co is indeed buried beneath the surface of the wafer. Comparison of the random and channeled yields of the Co distribution reveals that almost 50% of the as-implanted Co is substitutional at this temperature. The peak Co concentration is 27.5 atomic % and it appears at a depth of  $\sim 1150$  Å. A low-temperature furnace anneal (1 hour at 600°C) produces only slight changes in the Co profile, indicating some redistribution with little improvement in crystallinity. However, after an additional 1/2-hour anneal at 1000°C, the Co segregates into a layer that is still buried and has abrupt edges, the characteristic RBS yield for stoichiometric CoSi<sub>2</sub> (33.3 atomic %), and a greatly reduced channeling yield. The channeling yield of the Si itself is also reduced, but there is some evidence for interfacial damage. These data indicate good crystallin-

ity of both the buried silicide and the overlying Si.

The microstructural uniformity of this layer is shown in Fig. 4, a TEM cross-sectional view of the sample just described. This is a dark-field image that highlights the defects, but the uniformity of the layer is still striking. The surface Si, although defective, is crystalline, and some dislocation "loops" that result from annealing the end-of-range implant damage are apparent in the substrate. The imperfect lattice match results in misfit dislocations at the interfaces, but high-resolution TEM (see inset to Fig. 4) shows that they are smooth and abrupt. In fact, the interfaces are of very high quality for a silicide formed by such a brute-force technique.

The incorporation of the Co into the buried silicide layer is surprisingly complete, as determined by SIMS, which is more sensitive to low concentrations than RBS. This sample is difficult to study with mass spectroscopy because the Si isotopes overlap  $^{59}\text{Co}$ , but the results of a carefully calibrated measurement confirm that the Co concentration in the layer is that expected for  $\text{CoSi}_2$  and that the Co concentration in the surface and substrate Si is reduced by at least five orders of magnitude (the background level in the spectrometer). This result clearly illustrates the strength of the compound formation process.

A lower implant concentration of Co yields a narrower silicide layer buried under a correspondingly thicker surface Si layer, because the layers form at the peak of the implant profile. For example, a  $\text{Co}^+$  implant fluence of  $1.6 \times 10^{17}$  ions/cm $^2$  coalesces on annealing to a  $\text{CoSi}_2$  layer that is 600 Å thick and buried under 1100 Å of Si. However, when the total  $\text{Co}^+$  fluence is reduced by only 7% to  $1.5 \times 10^{17}$  ions/cm $^2$ , annealing no longer produces a uniform layer. This apparent threshold is even more obvious if the implant energy is reduced to 100 keV to reduce the straggle of the implant profile. In this case, a  $\text{Co}^+$  fluence of  $1 \times 10^{17}$  ions/cm $^2$  coalesces to a continuous silicide layer <400 Å thick. Again, however, a small reduction in implant concentration to  $0.9 \times 10^{17}$  ions/cm $^2$  gives an implanted profile that fails to coalesce on annealing. In this sample, the random profile does not change during annealing, but the channeling yield does decrease. Although the minimum total  $\text{Co}^+$  fluences that result in layer formation at 100 and 200 keV differ by almost 50%, the peak implant concentrations are very similar for the two energies. The data indicate that, for these conditions, the threshold Co concentration for layer formation is  $18.5 \pm 0.5$  atomic % (16). When these two samples are examined in TEM, the different morphologies are immediately discernible. The above-threshold sample does indeed yield a continuous single-crystal layer, whereas the below-threshold sample consists of oriented  $\text{CoSi}_2$  precipitates

interspersed with Si "holes." Similar results have been reported by Barbour *et al.* (24).

The structural integrity of these layers is reinforced by the electrical characteristics. If we plot the temperature dependence of the resistivity for several of these layers, the shapes of the curves are similar to those published by Hensel *et al.* (25) for comparable UHV-reacted  $\text{CoSi}_2$  films (Fig. 5); however, the curves are shifted downward. This is a manifestation of Matthiessen's rule: the resistivity due to lattice vibrations and the resistivity due to impurities and defects simply add (26). The similarity in the shape of the curves then implies that the layers are basically the same material, and the downward shift of the mesotaxy data indicates that these layers have a lower residual resistivity. We find that the best implanted silicide layers have residual resistivities that are lower by almost a factor of 2 than the best UHV-grown  $\text{CoSi}_2$  films and within a factor of 2 of the best bulk samples. In general, we found that, although the layers formed in (111) Si had lower channeling yields, those formed in (100) Si had lower residual resistivities.

Several important questions are raised by these results. What, for instance, causes the differences between the (100) and the (111) Si layers? Also, why are the electrical characteristics of the (100) layers so good? One possibility is that the reduced residual resistivities result from the inherent cleanliness of the ion implantation process. Both of the  $\text{CoSi}_2$  interfaces are buried, and, because the beam is mass selected, there are none of the contaminants (carbon, nitrogen, and oxygen) commonly thought to be present in conventional films. Another possibility is that the mesotaxy layers are closer to true stoichiometry, because formation occurs in a Si-rich environment without much mass transport. A deviation from stoichiometry in conventional silicides has been noted (27). The 1000°C anneal may also cause the marked improvement. Surface films tend to break apart at these temperatures—the buried layers seem to be more stable. Because  $\text{CoSi}_2$  is cubic, the electrical transport should be isotropic, so the observed differences in (100) and (111) Si layers are puzzling. We hypothesized that the differences may be due to strain; preliminary x-ray diffraction measurements indicate that there is indeed a difference in the degree of relaxation of the two layers (28).

The mesotaxy technique is not limited to  $\text{CoSi}_2$ . A guideline for choosing other silicides that might be suitable for mesotaxy can be found in the work of Ishiwara *et al.* (29). We have tried titanium, iron, chromium, nickel, and yttrium, observing oriented single-crystal growth in the last three. Madakson *et al.* (30) have reported polycrystalline  $\text{TiSi}_2$  layer formation;  $\text{CrSi}_2$  and  $\text{YSi}_2$  have a hexago-

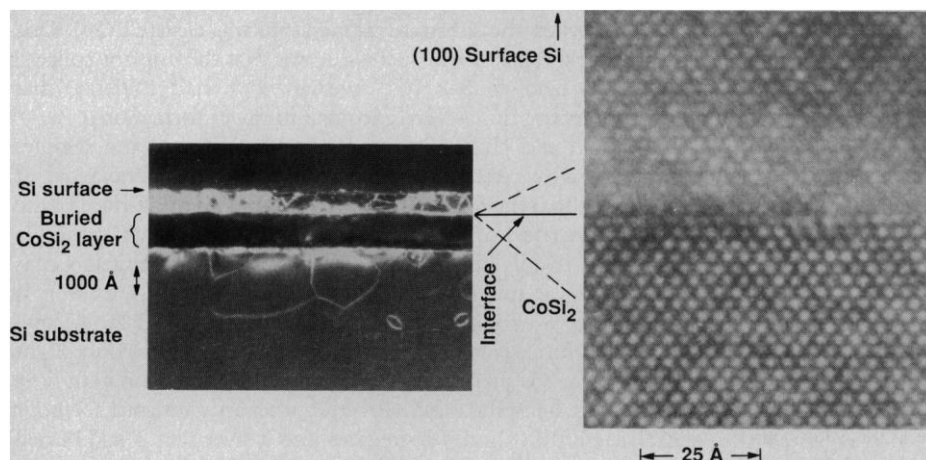
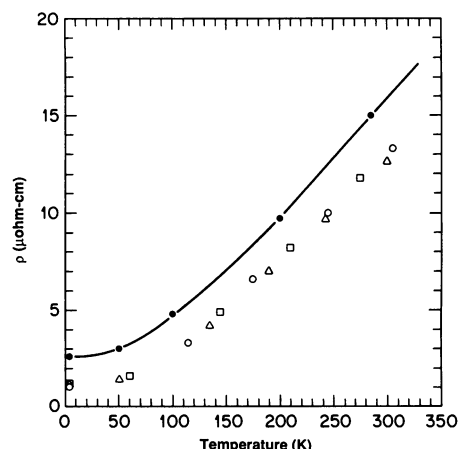


**Fig. 4 (left).** TEM micrograph of an 1100-Å single-crystal  $\text{CoSi}_2$  layer buried under  $\sim 600$  Å of surface Si. The high quality of the Si/ $\text{CoSi}_2$  interface is shown in the inset. [Reprinted from (16) with permission © Materials Research Society] **Fig. 5 (right).** Resistivity versus temperature charac-



teristics for several of the mesotaxy  $\text{CoSi}_2$  layers (triangles, open circles, and squares). Data of Hensel *et al.* (25) for UHV-deposited films (closed circles) are shown for comparison.

nal structure and therefore only grow in the (111) orientation of Si. Chromium disilicide is particularly interesting because it is thought to be a narrow-band gap semiconductor, although not much is known about its properties (31). Mesotaxy has made it possible to grow, for the first time, a continuous single-crystal layer of CrSi<sub>2</sub> (16, 32). The temperature dependence of such a layer shows that it is indeed semiconducting and can be distinguished from the surrounding Si. When the data are plotted in an Arrhenius fashion, an activation energy of 0.03 eV is extracted, far too small to be the intrinsic band gap. Hall effect measurements of the carrier concentration indicate that we are actually probing impurity levels in the band gap and experiments are under way to compensate these by doping with manganese.

## Summary

The formation of compounds by ion implantation and annealing is a powerful technique with some unexpected benefits. For buried oxide layers in SOI structures, implantation has the advantage that it is compatible with conventional Si processing and does not involve a melt. The coalescence of the implant profile to a buried layer also occurs for metal implants, as we have demonstrated with mesotaxy. In this case, the layers are not only single crystals aligned with the substrate, but they have very desirable electrical characteristics. We are currently trying to understand better the driving forces and perhaps the limits of this process. Some of the important growth parameters that have already emerged include adequate total implant concentration to achieve a threshold peak concentration, silicide stability to high-temperature annealing, and silicide lattice structure and mismatch with Si.

The success of the implantation technique has several implications. From the point of view of fundamental physics, the low residual resistivities of the metal layers indicate that the conduction electrons travel hundreds of angstroms (more than the thickness of the layer) between scattering events if the scattering from the near-perfect interfaces is specular. This effect makes the mesotaxy CoSi<sub>2</sub> layers potentially interesting for studying two-dimensional quantum transport effects. Moving to higher energy implantation (to get deeper layers with less surface damage) and optimizing the implant and annealing conditions should result in device-quality material. A Si/CoSi<sub>2</sub>/Si heterostructure fabricated in this way has possible application as a metal base transistor (where the electrons travel ballistically across the base region) if the layers can be made thinner than the electron mean free path (33). Furthermore, the depth of narrow silicide conductors formed by patterning the area of the implant (16) or using a focused ion beam (34) can be varied by changing the implant energy in order to cross under surface conductors in integrated circuit applications.

Looking to future research directions, we are confident that this technique is not limited to Si-based compounds or even to stable compounds. We have shown that implanting strontium into evaporated lanthanum/copper multilayers and then annealing results in the formation of a buried superconducting layer of (La<sub>1-x</sub>Sr<sub>x</sub>)<sub>2</sub>CuO<sub>7</sub> (35). This idea has been used for making superconducting YBa<sub>2</sub>-Cu<sub>3</sub>O<sub>x</sub> films by implantation of yttrium into multilayer films of barium and copper (36). Because high critical-temperature ( $T_c$ ) oxide superconductors are much more complicated multicomponent systems, it is not yet clear whether the formation process in these systems is the same as the ones we have discussed. We are exploring

ways to fabricate metastable phases of compounds by capitalizing on the nonequilibrium nature of the ion implantation process (37). The hope here is to capture a metastable phase of, for example, cupric oxide, CuO (interesting because of its apparently important role in the superconductivity of the high  $T_c$  oxides) by growing it inside Cu with O implantation.

## REFERENCES AND NOTES

1. L. Wegmann, in *Ion Implantation Science and Technology*, J. F. Ziegler, Ed. (Academic Press, New York, 1984), p. 3; S. Millman, Ed., *A History of Engineering and Science in the Bell System* (AT&T Bell Laboratories, New York, 1983), p. 289.
2. W. E. Beadle, J. C. C. Tsai, R. D. Plummer, Eds., *Quick Reference Manual for Silicon Integrated Circuit Technology* (Wiley, New York, 1985), p. 9-1.
3. A. G. Foyt, W. T. Lindley, C. M. Wolfe, J. P. Donnelly, *Solid State Electron.* **12**, 209 (1969); D. V. Morgan and F. H. Eisen, in *Gallium Arsenide*, J. Howes and D. V. Morgan, Eds. (Wiley, New York, 1985), p. 161 and references therein.
4. J. S. Williams, R. G. Elliman, W. L. Brown, T. E. Seidel, *Phys. Rev. Lett.* **55**, 1482 (1985); D. C. Jacobson *et al.*, *Mater. Res. Soc. Symp. Proc.* **74**, 327 (1987).
5. B. R. Appleton, in *Ion Implantation and Beam Processing*, J. S. Williams and J. M. Poate, Eds. (Academic Press, New York, 1984), p. 189.
6. I. L. Singer, *Appl. Surf. Sci.* **18**, 28 (1984).
7. G. Deamaley, J. H. Freeman, R. S. Nelson, J. Stephen, *Ion Implantation* (North-Holland, Amsterdam, 1973).
8. J. F. Ziegler, J. P. Biersack, U. Littmark, in *The Stopping and Range of Ions in Solids*, J. F. Ziegler, Ed. (Pergamon, New York, 1985), vol. 1.
9. L. C. Feldman and J. W. Mayer, *Fundamentals of Surface and Thin Film Analysis* (North-Holland, New York, 1986).
10. M. H. Badawi and K. V. Anand, *J. Phys. D* **10**, 1931 (1977).
11. K. Izumi, M. Doken, H. Ariyoshi, *Electron Lett.* **14**, 593 (1978).
12. P. L. F. Hemment, *Mater. Res. Soc. Symp. Proc.* **53**, 207 (1986) and references therein.
13. See, for instance, articles in *Mater. Res. Soc. Symp. Proc.* **53** (1986).
14. C.-E. D. Chen and Radiation Hard SOI Project Team, *Mater. Res. Soc. Symp. Proc.* **107**, 309 (1988).
15. A. E. White *et al.*, *Appl. Phys. Lett.* **50**, 19 (1987).
16. A. E. White *et al.*, *Mater. Res. Soc. Symp. Proc.* **100**, 3 (1988).
17. A. H. van Ommen, H. J. Ligthart, J. Politiek, M. P. A. Vieggers, *ibid.* **93**, 119 (1987).
18. S. Maeyama and I. Kajiyama, *Jpn. J. Appl. Phys.* **21**, 744 (1982); T. Tsujide, M. Nojiri, H. Kitagawa, *J. Appl. Phys.* **51**, 1605 (1980).
19. S. P. Murarka, *Silicides for VLSI Applications* (Academic Press, New York, 1983).
20. R. T. Tung, J. M. Gibson, J. M. Poate, *Appl. Phys. Lett.* **42**, 888 (1983); B. D. Hunt *et al.*, *Mater. Res. Soc. Symp. Proc.* **56**, 151 (1986); R. T. Tung, J. M. Gibson, A. F. J. Levi, *Appl. Phys. Lett.* **48**, 1264 (1986).
21. A. E. White *et al.*, *Appl. Phys. Lett.* **50**, 95 (1987).
22. P. Sigmund, *Phys. Rev.* **184**, 383 (1969); Z. L. Liao and J. W. Mayer, *J. Vac. Sci. Technol.* **15**, 1629 (1978).
23. F. H. Sanchez, F. Namavar, J. I. Budnick, A. Fashihudin, H. C. Hayden, *Mater. Res. Soc. Symp. Proc.* **51**, 439 (1986); G. J. Campisi, H. B. Dietrich, M. Delfino, B. K. Sadana, *ibid.* **54**, 747 (1986).
24. J. C. Barbour, S. T. Picraux, B. L. Doyle, *Mater. Res. Soc. Symp. Proc.* **107**, 269 (1988).
25. J. C. Hensel, R. T. Tung, J. M. Poate, F. C. Unterwald, *Appl. Phys. Lett.* **44**, 913 (1984).
26. C. Kittel, *Introduction to Solid State Physics* (Wiley, New York, 1976), p. 171.
27. P. V. Geld and F. A. Sidorenko, *Silitsidi Perekhodnikh Metallov Chervetogo Perioda* (Izdatelstvo "Metallurgiya," Moscow, 1971).
28. J. M. Vandenberg, A. E. White, K. T. Short, J. M. Gibson, in preparation.
29. H. Ishiwara, S. Saitoh, K. Hikosaka, *Jpn. J. Appl. Phys.* **20**, 843 (1981).
30. P. B. Madakson, G. C. Clark, F. Legoues, J. E. E. Baglin, *Mater. Res. Soc. Symp. Proc.* **107**, 281 (1988).
31. D. Shinoda, S. Asanabe, Y. Sasaki, *J. Phys. Soc. Jpn.* **19**, 269 (1964); I. Nishida and T. Sakati, *J. Phys. Chem. Solids* **39**, 499 (1978).
32. A. E. White, K. T. Short, R. C. Dynes, J. P. Garno, J. M. Gibson, *Mater. Res. Soc. Symp. Proc.* **74**, 481 (1987).
33. J. C. Hensel, *ibid.* **54**, 499 (1986).
34. W. L. Brown, in *Erosion and Growth of Solids Stimulated by Atom and Ion Beams*, vol. 112 in the North Atlantic Treaty Organization Advanced Study Institutes Series in Applied Science, G. Kiriakios, G. Carter, J. L. Whitton, Eds. (Nijhoff, Boston, 1986), p. 338.
35. K. T. Short *et al.*, *Bull. Am. Phys. Soc.* **33**, 779 (1988).
36. M. Nastasi *et al.*, *Appl. Phys. Lett.* **52**, 1729 (1988).
37. A. E. White and K. T. Short, in preparation.
38. The work reported here was done in collaboration with R. C. Dynes, D. C. Jacobson, J. M. Poate, L. N. Pfeiffer, J. M. Gibson, R. Hull, J. L. Batstone, J. M. Vandenberg, J. P. Garno, F. C. Unterwald, K. W. West, F. A. Stevie, and P. M. Kahora, all at AT&T Bell Laboratories. In addition, we benefited greatly from discussions with R. T. Tung, W. L. Brown, A. F. J. Levi, and S. J. Pearton. We thank A. D. White for a critical reading of the manuscript.